Possibility of using Zn as the quantum absorber for a laser-cooled neutral atomic optical frequency standard

Guangfu Wang and Anpei Ye*

Institute of Quantum Electronics, School of Electronics Engineering and Computer Science, Peking University, Beijing 100871, People's Republic of China

(Received 18 May 2007; published 9 October 2007)

In this paper, we present a detailed investigation of the laser cooling and trapping of the Zn atom, and various schemes employing the $^1S_0$-$^3P_0$ transition, induced by nuclear magnetic moment or applied fields, as the clock transition. Using numerical simulations, the deceleration of Zn by a Zeeman slower and its capture by a magneto-optical trap (MOT) are analyzed, and the corresponding parameters are determined. The linear loss rate and the coefficient for two-body collisional loss in the MOT are discussed. To prove the feasibility of the intercombination line cooling, one-dimensional semiclassical Monte Carlo simulations are performed. Multiconfiguration Hartree-Fock and multiconfiguration Dirac-Fock approaches are employed to calculate the hyperfine-induced $^1S_0$-$^3P_0$ transition. Up to now, various schemes inducing the $^1S_0$-$^3P_0$ transition in bosonic isotopes have been proposed for alkaline-earth-metal atoms and Yb. Their applicability for Zn are investigated, and the corresponding parameters of Zn are calculated. Our results show that the Zn atom, either fermionic or bosonic, is a potential candidate for the quantum absorber used in laser-cooled neutral atomic optical frequency standard.

DOI: 10.1103/PhysRevA.76.043409 PACS number(s): 32.80.Pj, 42.62.Eh, 31.30.Gs, 32.80.Qk

I. INTRODUCTION

Atomic clocks have been applied widely in both fundamental scientific researches and technologies, such as testing stability of fundamental constants, broadband communication networks, and global positioning systems (GPS). Though the SI second is currently realized by the microwave-based Cs atomic clock with an uncertainty of 10^{-15}, optical clocks based on single trapped ions [1] or laser-cooled neutral atoms [2,3] have the potential to outperform it in the near future due to the high frequency and correspondingly high resonance quality factors. The single trapped ion approach is well known to have a better ultimate frequency accuracy due to the perfect confining of the ion motion. However, the laser-cooled neutral atom approach can provide a large signal-to-noise ratio, and thus a better frequency stability. Furthermore, the recent scheme trapping neutral atoms in the Lamb-Dicke regime in an optical lattice [2] has made the atom approach have the advantage of the ion approach as well. Therefore, neutral atom approach is expected to do better than the ion approach. In the laser-cooled neutral atom approach, quantum absorbers are usually performed by alkaline-earth-metal atoms and Yb, an alkaline-earth-metal-like element. There are a large number of papers, both experimental and theoretical, referring to them [2–4]. In contrast, although group IIB atoms are also alkaline-earth-metal-like atoms, there is almost no literature discussing whether they can serve in a laser-cooled neutral atomic frequency standard. The actualities motivate us to investigate this problem in detail. In this paper, we explore the possibility of laser-cooled neutral atomic optical frequency standard using the Zn atom, the simplest atom of group IIB. As we know, the atoms that serve as quantum absorbers in a laser-cooled neutral atomic clock should have two elements, the cooling and the clock transitions. Therefore, we investigate the possibility from these two aspects. Since, to the best of our knowledge, there is no experimental implement of laser cooling and trapping of Zn available, we first analyze it theoretically in Sec. II. Then, in Sec. III we calculate the linewidth of the hyperfine-induced $^1S_0$-$^3P_0$ transition in ^{67}Zn, which is employed as the clock transition. Up to now, some clock schemes have been proposed to employ $^1S_0$-$^3P_0$ transition in bosonic isotopes of alkaline-earth-metal-like atoms. In Sec. IV, we investigate the feasibility of these schemes for Zn.

II. LASER COOLING AND TRAPPING OF Zn

For reducing the Doppler effect and increasing interaction time, cooling of interrogated absorbers in an atomic frequency standard is generally necessary. For atomic absorbers, the most widely used approach is to employ a magneto-optical trap (MOT), which can implement both cooling and trapping simultaneously. However, since the capture velocity of a MOT is limited, a Zeeman slower (ZS) is usually employed to decelerate the hot atoms ejected from an oven before they get into the MOT.

Compared with alkaline-earth metals and Yb, Zn has a relative low melting point (693 K). This implies that a comparable vapor pressure can be obtained with a lower oven temperature than alkaline-earth metals and Yb. When the temperature is between 298 K and 693 K, the saturated vapor pressure of Zn can be estimated approximately using the following equation [5]:

$$\log(P) = -6850/T - 0.755 \log T + 11.24, \qquad (1)$$

where P is the vapor pressure in torr and T in K. If a saturated vapor pressure of 5×10^{-6} torr, as in [6], is desired, the

*yap@pku.edu.cn

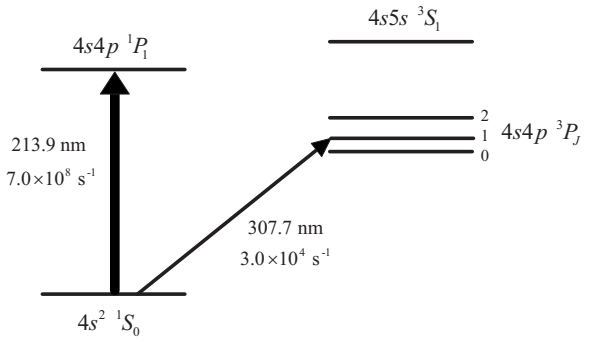

FIG. 1. Some lowest-lying energy levels of Zn with the strong line $^1S_0$-$^1P_1$ and the intercombination line $^1S_0$-$^3P_1$. The wavelengths of the transition are those in vacuum. Einstein A coefficients are also shown.

oven temperature is only about 473 K. In this case, the root-mean-square (RMS) velocity is about 420 m/s.

Partial low-lying energy levels of Zn are shown in Fig. 1. The level structure is similar to alkaline-earth-metal atoms. When atoms ejected from the oven pass through the ZS, the strong line $^1S_0$-$^1P_1$ can be employed to decelerate them. Because of the large decay width ($\Gamma=2\pi\times 112$ MHz) and the short wavelength ($\lambda=213.9$ nm), the saturation intensity I_s of this line is very large. The value is about 1.50 W/cm^2, which is a few tens of times larger than Ca, Sr, and Yb. It seems that the intensity of deceleration light should be large as well. However, because of the same reason, a sufficient force can be offered with a small on-resonant saturation parameter s_0 ($s_0=I/I_s$). When the intensity of deceleration light is 60 mW/cm^2, s_0 is about 0.04, and the on-resonant deceleration is [7]

$$a=\frac{\hbar k\Gamma}{2M}\frac{s_0}{1+s_0}=3.85\times 10^5 \text{ m/s}^2, \tag{2}$$

where $k=2\pi/\lambda$ is the wave vector and M is the mass of the atom (the average atomic mass is used here). This is comparable with Sr and Yb [6] when the same intensity is used. If the capture velocity is 420 m/s and the final velocity is 40 m/s, the length of the ZS will be 22.7 cm, which is acceptable. To reduce the affect of the deceleration light when atoms exit out of the ZS, the σ^- ZS scheme [8] is preferred, where the detuning of deceleration light is large and the magnetic field is increased along the axis of the atomic beam. Once atoms exit out of the solenoid, the deceleration light will be far from resonance with them. In our case, the detuning of the deceleration laser is −1964 MHz, and the profile of the magnetic field is given as

$$B(z)=B_0\left(1-\sqrt{1-\frac{z}{z_0}}\right), \tag{3}$$

where $B_0=1403$ G, $z_0=22.91$ cm, and z is the axial distance in units of cm. A numerical simulation (Fig. 2) shows that our design of the ZS can meet the requirement well.

After atoms pass through the ZS and get into the region of the MOT, they still have a velocity of a few tens of m/s. To trap these atoms, MOT must be able to stop them before they

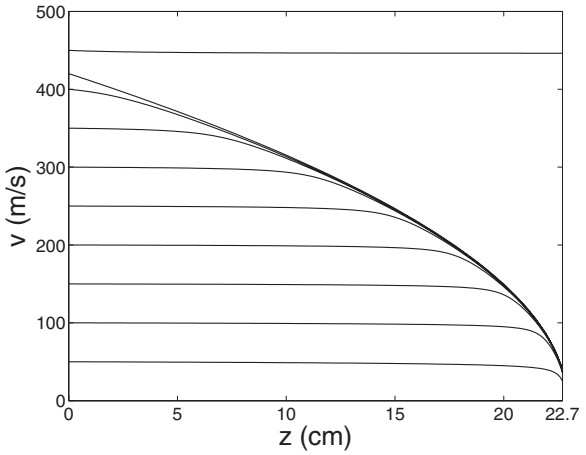

FIG. 2. Numerical simulation of the deceleration process of the ZS. Zn atoms with a velocity smaller than 420 m/s will be decelerated to 40 m/s when they pass through the ZS.

reach the opposite side of the region. In our case, the capture velocity of the MOT should be larger than 40 m/s. To determine the parameters of the MOT, we calculated the dependence of the capture velocity on the laser detuning and the magnetic field gradient in a one-dimensional (1D) model. In our calculation, we assumed that each laser beam had an intensity of 10 mW/cm^2 and a diameter of 20 mm. The results are shown in Fig. 3(a). It can be seen that there is an approximate triangle region where a capture velocity larger than 40 m/s can be obtained by arbitrary combination of the laser detuning $\Delta\nu_L$ and the magnetic field gradient dB/dx. For example, when $\Delta\nu_L$ is −140 MHz and dB/dx is 70 G/cm, all atoms with a velocity below 48 m/s will be captured [see Fig. 3(b)]. After a process of damping oscillation, these atoms will be trapped in the centric part of the MOT.

The storage time of the MOT and the density of atoms trapped in it can be determined by the trap loading equation

$$\frac{dn}{dt}=L_n-Rn-\beta n^2, \tag{4}$$

where n is the density, L_n is the loading rate, R is the linear loss rate, and β is the coefficient for two-body collisional loss. In Ca, Sr, and Yb atoms, there is an empty $(n-1)d$ subshell. One of the valence electrons can occupy this subshell with a relatively lower energy. That makes these atoms have some D levels lying below the $nsnp$ $^1P_1$. For these elements, the loss channels due to the weak transitions $^1P_1\rightarrow D\rightarrow {}^3P$ are the main contribution to the linear loss rate. That restricts the population of atoms trapped in the MOT and the storage time of the MOT. To decrease the loss rate, repumping lasers must be added [9,10]. Compared to Ca, Sr, and Yb, Zn atoms have a full $(n-1)d$ subshell and there is no D level below the $nsnp$ $^1P_1$. Therefore, the loss channels $^1P_1\rightarrow D\rightarrow {}^3P$ do not exist. The decay rates of direct transitions from $^1P_1$ to $^3P_{0,2}$ are only in an order of 10^{-2} s^{-1}, which is far smaller than the linear loss rate of Ca, Sr, and Yb. However, electrons of the $(n-1)d$ subshell cannot screen the nuclear charge effectively, which leads to large level in-

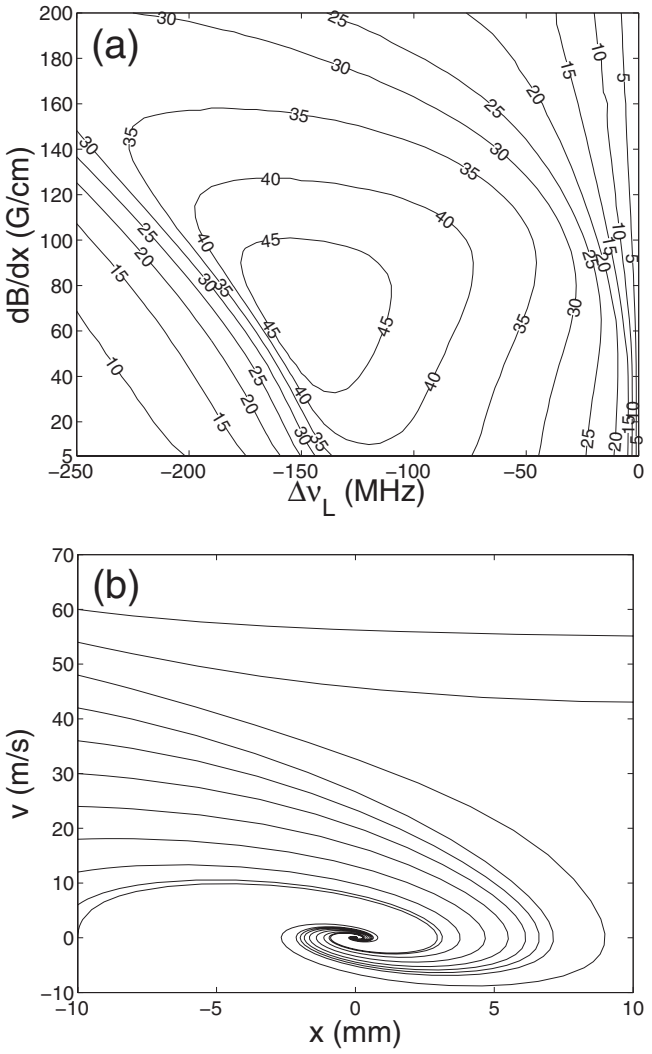

FIG. 3. (a) Contour map to show the dependence of the capture velocity on the laser detuning and the magnetic field gradient. In the map, there is an approximate triangle region where the capture velocity is larger than 40 m/s. (b) Numerical simulation of the capture process of the MOT. When $\Delta\nu_L=-140$ MHz and $dB/dx=70$ G/cm, Zn atoms with a velocity below 48 m/s will be captured by the MOT and collected in the center.

tervals. For Zn atom, the interval between $^1P_1$ and $^1S_0$ is so large that an atom at the $^1P_1$ state can be ionized by absorbing another photon of the trapping laser. Therefore, in Zn atom, there is a loss channel due to photoionization that does not exist in Ca, Sr, and Yb. The loss rate is approximated by

$$R_p = \frac{s_0/2}{1+s_0+4(\Delta\nu_L/\Gamma)^2} I_t \sigma_{pt}, \tag{5}$$

where the first factor on the right-hand side is the population of the $^1P_1$ state, I_t is the total intensity of the six trapping beams, $s_0=I_t/I_s$ is the on-resonant saturation parameter, $\Delta\nu_L$ is the laser detuning, and σ_{pt} is the total photoionization cross section. Since there is no autoionization state resonating with the trapping laser, the photoionization rate is small. A simple run of Cowan's code [11] shows that the total photoionization cross section is less than 1.0×10^{-17} cm^2. In our case, the total intensity is 60 mW/cm^2 [$\approx 6.5\times10^{16}$ photons/(cm^2 s)], therefore the loss rate will be less than 10^{-2} s^{-1}, which is also far smaller than the loss rate due to $^1P_1\rightarrow D\rightarrow{}^3P$ transitions in Ca, Sr, and Yb.

Another linear loss channel is caused by collisions between trapped Zn atoms and background gas, which is mainly hot Zn atoms. Since most of the trapped atoms are in the ground state, only ground-state collisions between trapped atoms and background gas are considered. The leading term of the potential between two ground-state Zn atoms at long range is the van der Waals interaction. It arises from the interaction between induced dipole moments and is given by

$$V(R) = -C_6/R^6, \tag{6}$$

where dispersion coefficient C_6 is 282 a.u. ($=2.70\times10^{-77}$ J m^6) [12] and R is the distance between atoms. In this form of potential, the total collisional cross section is [13,14]

$$\sigma_{ct} = \alpha(C_6/\hbar v_b)^{2/5}, \tag{7}$$

where $\alpha=8.083$, and v_b is the velocity of the impinging background gas atom. In the case of small-angle collisions, trapped atoms may not gain sufficient kinetic energy to be ejected from the trap. Therefore, the cross section related to the loss of trapped atoms is usually less than σ_{ct} by a few tenths [13]. However, for simplicity, we do not consider this difference here, and as an upper bound, the collisional loss rate is given by

$$R_c = n_b v_b \sigma_{ct}, \tag{8}$$

where n_b and v_b are the density and the velocity of background gas atoms, respectively. When the background gas is at room temperature, $T=300$ K, and has a vacuum level of 10^{-8} torr, σ_{ct} and R_c are 722 Å^2 and 0.8 s^{-1}, respectively. The dispersion coefficient of Zn is smaller than that of alkaline-earth-metal atoms [15]. Therefore, in the same condition, Zn has a smaller collisional loss rate than alkaline-earth-metal atoms.

To estimate the coefficient for two-body collisional loss, we employ the semiclassical model described in [16]. In that model, with the approximation of zero initial kinetic energy for the atom pair and unit loss probability for the pair surviving to a small distance, β is given by

$$\beta = \int_0^\infty dR_0 4\pi R_0^2 P_e(R_0) S(R_0), \tag{9}$$

where $4\pi R_0^2$ term gives the number distribution at a distance R_0 from the target atom, $P_e(R_0)$ is the excitation rate at separation R_0, and $S(R_0)$ is the probability of the atom pair surviving in the excited state until colliding at $R\sim0$. The excitation rate is given by

$$P_e(R_0) = \frac{I}{\hbar\omega_L}\frac{\lambda^2}{2\pi}\left(\frac{[\Gamma_m(R_0)/2]^2}{[\Gamma_m(R_0)/2]^2+\Delta(R_0)^2}\right), \tag{10}$$

where I and ω_L are the laser excitation intensity and frequency, $\Gamma_m(R_0)$ is the molecular decay rate for separation R_0,

$\Delta(R_0)=\omega_0-\omega_L-C_3/\hbar R_0^3$ is the detuning from the molecular resonance frequency. The survival probability is given by

$$S(R_0)=\exp\left(-\sqrt{\frac{\mu R_0^5}{2C_3}}\int_0^1\frac{\Gamma_m(x)dx}{\sqrt{x^{-3}-1}}\right), \tag{11}$$

where μ is the reduced mass of the colliding pair, $x=R/R_0$. When $R<\lambda\!\!\!^{-}$ ($\lambda\!\!\!^{-}=\lambda/2\pi$), the molecular decay rates of $^1\Sigma_u^+$ and $^1\Pi_g$, the two states with an attractive potential, are approximated, respectively, by

$$\Gamma_\Sigma(R)=2\Gamma_a,\quad \Gamma_\Pi(R)=\frac{\Gamma_a}{5}\left(\frac{R}{\lambda\!\!\!^{-}}\right)^2, \tag{12}$$

where Γ_a is the atomic decay rate. Their errors are both about 5% at $R=\lambda\!\!\!^{-}$. For $^1\Sigma_u^+$ state, using (12) and $C_3=4.42\times10^{-48}$ J m^3, the survival factor can be written as

$$S_\Sigma(R_0)=\exp[-(R_0/R_s)^{5/2}]=\exp[-(\delta_s/\delta)^{5/6}], \tag{13}$$

where $\delta=C_3/\hbar R_0^3$, $R_s=108$ Å, and $\delta_s=5.3$ GHz. Therefore, (9) can be written as

$$\beta_\Sigma(\delta_L,I)=4.2\times10^{-10}I\int_0^\infty dx\frac{x^{-2}\exp(-x^{-5/6})}{1+a^2(x-\delta_L/\delta_s)^2}, \tag{14}$$

where I is the trap intensity in W/cm^2, $x=\delta/\delta_s$, $a=47$, δ_L is the laser detuning from the atomic resonance, and β is in units of cm^3/s. For the $^1\Pi_g$ state, $C_3=2.21\times10^{-48}$ J m^3 and the survival factor can be written as

$$S_\Pi(R_0)=\exp[-(R_0/R_s)^{9/2}]=\exp[-(\delta_s/\delta)^{3/2}], \tag{15}$$

where $R_s=301$ Å, $\delta_s=122$ MHz, and then

$$\beta_\Pi(\delta_L,I)=9.0\times10^{-9}I\int_0^\infty dx\frac{x^{-2}\exp(-x^{-3/2})}{1+a(x-\delta_L/\delta_s)^2x^{4/3}}, \tag{16}$$

where $a=192$. The results are shown in Fig. 4 (dashed lines).

In the above calculation, we have supposed $R<\lambda\!\!\!^{-}$. However, since $\lambda\!\!\!^{-}$ of Zn is only 34.0 nm, this condition may not be tenable when the laser detuning is less than 170 MHz for the $^1\Sigma_u^+$ state and 85 MHz for the $^1\Pi_g$ state. When $R>\lambda\!\!\!^{-}$, (12) will not be accurate sufficiently. Higher order terms should be included in the expressions of the molecular decay rate. If only the two lowest order terms are retained, we can write the following [17]:

$$\Gamma_\Sigma(R)=\Gamma_a\left[2-\frac{1}{10}\left(\frac{R}{\lambda\!\!\!^{-}}\right)^2\right], \tag{17}$$

$$\Gamma_\Pi(R)=\Gamma_a\left[\frac{1}{5}\left(\frac{R}{\lambda\!\!\!^{-}}\right)^2-\frac{3}{280}\left(\frac{R}{\lambda\!\!\!^{-}}\right)^4\right]. \tag{18}$$

Even when $R=2\lambda\!\!\!^{-}$, the errors of (17) and (18) are still less than 4%. In this case, for the $^1\Sigma_u^+$ state, the survival factor should be modified as

$$S_\Sigma(R_0)=\exp[-(\delta_s/\delta)^{5/6}+(\delta_s'/\delta)^{3/2}], \tag{19}$$

where $\delta_s'=122$ MHz. Then, β should be modified as

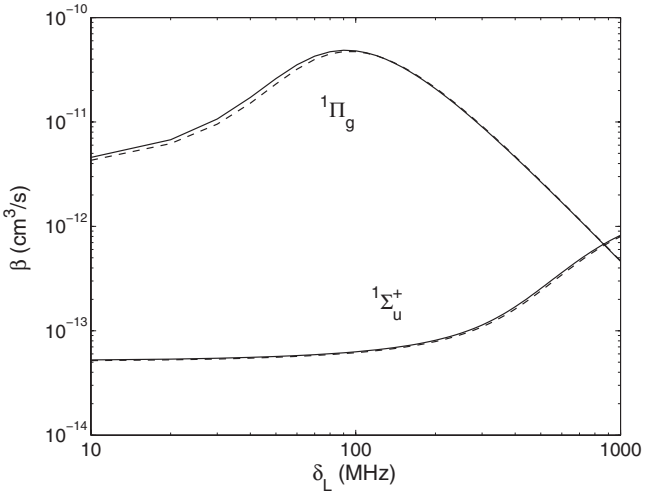

FIG. 4. The dependence of the two-body collisional loss rate coefficients for excitations to the $^1\Pi_g$ and $^1\Sigma_u^+$ molecular state on δ_L. The trap intensity is 60 mW/cm^2. Here δ_L is defined as in [16], and is equal to $-\Delta\nu_L$.

$$\beta_\Sigma(\delta_L,I)=4.2\times10^{-10}I\times\int_0^\infty dx\frac{x^{-2}\exp(-x^{-5/6}+kx^{-3/2})}{1+a^2(x-\delta_L/\delta_s)^2(1-px^{-2/3})^{-2}}, \tag{20}$$

where $p=5.1\times10^{-3}$ and $k=3.5\times10^{-3}$. Similarly, for the $^1\Pi_g$ state, the survival factor should be rewritten as

$$S_\Pi(R_0)=\exp[-(\delta_s/\delta)^{3/2}+(\delta_s'/\delta)^{13/6}], \tag{21}$$

where $\delta_s'=26$ MHz. Then, β becomes

$$\beta_\Pi(\delta_L,I)=9.0\times10^{-9}I\times\int_0^\infty dx\frac{x^{-2}\exp(-x^{-3/2}+kx^{-13/6})}{1+a(x-\delta_L/\delta_s)^2x^{4/3}(1-px^{-2/3})^{-2}}, \tag{22}$$

where $p=4.2\times10^{-2}$ and $k=3.4\times10^{-2}$. The modified results are also shown in Fig. 4 (solid lines). Since parameters k and p are small for both states, the modifications are not remarkable. The difference becomes visible only when detuning is less than 85 MHz for the $^1\Pi_g$ state. The curve profiles of trap loss coefficients versus detuning are similar to Sr, but the values are more than one order smaller for the same laser intensity and detuning.

From the above calculations, we can see that both the linear loss rate and the two-body collisional loss rate coefficients of Zn are smaller than Sr. Therefore, long storage time and large trapped population can be obtained easily without requiring repumping lights.

In the above conditions ($s_0=0.04$, $\Delta\nu_L=-140$ MHz), the Doppler limit of Zn is 4 mK. For fermionic isotopes, Sisyphus cooling mechanism may cool them further to μK temperatures, which we will not discuss in this paper, but for bosonic isotopes, the Sisyphus cooling scheme will not work since their ground states have only one sublevel. However,

some schemes based on Doppler cooling have been proposed to cool alkaline-earth-metal-like atoms down to μK after they have been cooled in a first stage, such as intercombination line [6,9,18], quenching [19,20], and two-photon Doppler cooling [21]. The linewidth of the $^1S_0$-$^3P_1$ transition of Zn is $2\pi\times 4.71$ kHz, which is comparable with Sr. Therefore, we need not use those complicated multiphoton cooling schemes. The simple scheme using this intercombination line will work in a second stage cooling. We have performed 1D semiclassical Monte Carlo simulations to prove its feasibility. Since the real temperature of cooled atoms is usually higher than the Doppler limit, in our simulations, we assumed the initial temperature of Zn atoms is 8 mK. This implies that their initial RMS velocity and position are 1.0 m/s and 0.67 mm, respectively. To compensate for the small velocity capture range due to the narrow linewidth, broadband laser, pulsed [19] or frequency modulated [9,18], should be used. In our simulations, the laser had a central frequency tuned 1.6 MHz below the $^1S_0$-$^3P_1$ resonance, and in each side of the central frequency, there were 60 sidebands with a interval of 25 kHz. For simplicity, we assumed that the intensities of the sidebands were equal, and their linewidth was neglected compared with the $^1S_0$-$^3P_1$ line. Our simulations with 1000 atoms and a time grid of 10 μs show that when the intensity of each beam is 5 mW/cm^2 and the magnetic field gradient is 2 G/cm, 60% of the atoms can be cooled to the recoil limit in 40 ms (Fig. 5). Increasing the frequency range of the laser can cool more atoms with a larger velocity, but it is difficult to cool them effectively to the recoil limit without increasing the laser intensity. Decreasing the magnetic field gradient can also increase the efficiency of the second stage cooling, however, more time will be required to pull atoms back to the center. After atoms have been loaded to the intercombination line MOT, magnetic field gradient can be increased to achieve higher density, and the frequency modulation can be turned off to operate at a single frequency.

III. HYPERFINE-INDUCED TRANSITION IN ^{67}Zn

In earlier optical standards using alkaline-earth-metal elements, spin-forbidden transition $^1S_0$-$^3P_1$ is employed as the clock transition. However, the linewidth of this transition in Sr and Yb is so large as to lead a low Q-value. Furthermore, a nonzero electronic angular momentum make the transition frequency sensitive to the polarization of the laser field, such as the optical lattice. Therefore, more and more attention has been focused on the $^1S_0$-$^3P_0$ transition. Since the linewidth of the $^1S_0$-$^3P_1$ transition in Zn is almost as large as Sr, we also propose the $^1S_0$-$^3P_0$ transition (λ=309.5 nm) of ^{67}Zn ($I=5/2$, $\mu_I=0.875\ 15\mu_N$) as the clock transition.

In bosonic isotopes, the $^1S_0$-$^3P_0$ transition is completely forbidden, but in fermionic isotopes, a weak transition is induced by the nuclear magnetic dipole moment. Using the first-order perturbation theory, the wave function corresponding to $4s4p\ ^3P_0IF$ ($F=I$) state can be written

$$|4s4p\ ^3P_0IF\rangle^{(1)} = |4s4p\ ^3P_0IF\rangle + \sum_{\gamma'} a_{\gamma'}|\gamma' IF'\rangle, \quad (23)$$

where

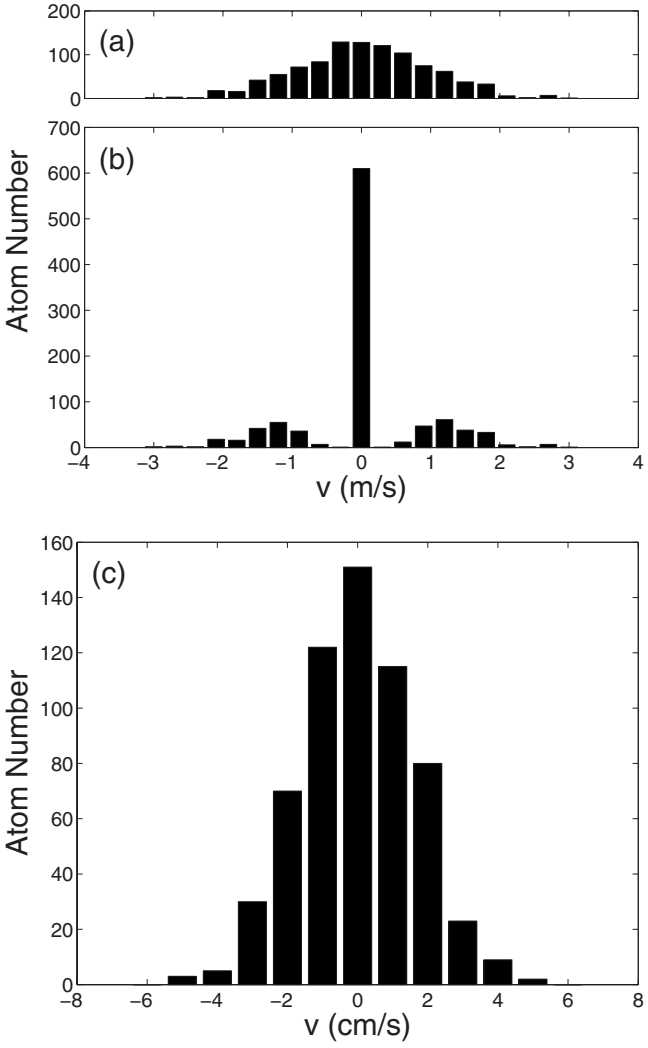

FIG. 5. Results of Monte Carlo simulations showing velocity distribution of Zn atoms (a) before and (b), (c) after 40 ms intercombination cooling. 60% of 1000 atoms are trapped and cooled (b), and their RMS velocity is the recoil velocity 2 cm/s (c).

$$a_{\gamma'} = \frac{\langle \gamma' IF'|H_{\rm hfs}|4s4p\ ^3P_0IF\rangle}{E(4s4p\ ^3P_0) - E(\gamma')}, \quad (24)$$

$F'=I$, and $H_{\rm hfs}$ is the hyperfine interaction Hamiltonian. Generally, only the two lowest-order terms are considered, and $H_{\rm hfs}$ can be written as [22]

$$H_{\rm hfs} = \mathbf{T}^{(1)} \cdot \mathbf{M}^{(1)} + \mathbf{T}^{(2)} \cdot \mathbf{M}^{(2)}, \quad (25)$$

where $\mathbf{T}^{(k)}$ and $\mathbf{M}^{(k)}$ are spherical tensor operators of rank k in the electronic and nuclear spaces, respectively. The $k=1$ term of the expansion represents the magnetic dipole interaction and the $k=2$ term the electric quadrupole interaction. In the summation of (23), only the intermediate states which can be connected with ground state by an electric dipole transition are included. The total electronic angular momentums J' of these states are all one. Since the total electronic angular momentum J of the $4s4p\ ^3P_0$ state is zero, the con-

tribution of the electric quadrupole interaction will be null, i.e.,

$$\langle \gamma' IF' | \mathbf{T}^{(2)} \cdot \mathbf{M}^{(2)} | 4s4p\ ^3P_0 IF \rangle = 0. \tag{26}$$

Therefore,

$$\langle \gamma' IF' | H_{\rm hfs} | 4s4p\ ^3P_0 IF \rangle = \sqrt{I(I+1)} A(\gamma', 4s4p\ ^3P_0), \tag{27}$$

where $A(\gamma', 4s4p\ ^3P_0)$ is the off-diagonal magnetic dipole constant written as

$$A(\gamma', 4s4p\ ^3P_0) = \frac{\mu_I}{I} \frac{1}{\sqrt{6}} \langle \gamma' \| \mathbf{T}^{(1)} \| 4s4p\ ^3P_0 \rangle. \tag{28}$$

The transition rate for $4s4p\ ^3P_0 \rightarrow 4s^2\ ^1S_0$ is

$$A_{\rm hfs} = \frac{4}{3} \alpha^3 [E(4s4p\ ^3P_0) - E(4s^2\ ^1S_0)]^3 \frac{S}{2I+1}, \tag{29}$$

where α is the fine-structure constant and the line strength S is given by

$$S = |\langle 4s^2\ ^1S_0 IF \| D \| 4s4p\ ^3P_0 IF \rangle^{(1)}|^2. \tag{30}$$

Substituting Eqs. (23), (24), and (27) for Eq. (30), S can be written as

$$S = I(I+1) \left| \sum_{\gamma'} \frac{\langle 4s^2\ ^1S_0 IF \| D \| \gamma' IF' \rangle A(\gamma', 4s4p\ ^3P_0)}{E(4s4p\ ^3P_0) - E(\gamma')} \right|^2. \tag{31}$$

Using Eq. (31) and the relations

$$A(\gamma' \rightarrow 4s^2\ ^1S_0) = \frac{4}{3} \alpha^3 [E(\gamma') - E(4s^2\ ^1S_0)]^3 \frac{|\langle 4s^2\ ^1S_0 \| D \| \gamma' \rangle|^2}{3}, \tag{32}$$

$$|\langle 4s^2\ ^1S_0 IF \| D \| \gamma' IF' \rangle| = \sqrt{\frac{2I+1}{3}} |\langle 4s^2\ ^1S_0 \| D \| \gamma' \rangle|, \tag{33}$$

$A_{\rm hfs}(4s4p\ ^3P_0 \rightarrow 4s^2\ ^1S_0)$ can be written as

$$A_{\rm hfs} = I(I+1) \times \left| \sum_{\gamma'} \varepsilon_{\gamma'} p_{\gamma'} \frac{\sqrt{A(\gamma' \rightarrow 4s^2\ ^1S_0)} A(\gamma', 4s4p\ ^3P_0)}{E(4s4p\ ^3P_0) - E(\gamma')} \right|^2, \tag{34}$$

where

$$\varepsilon_{\gamma'} = \left[\frac{E(4s4p\ ^3P_0) - E(4s^2\ ^1S_0)}{E(\gamma') - E(4s^2\ ^1S_0)} \right]^{3/2}, \tag{35}$$

and $p_{\gamma'}$ is a phase factor to indicate the sign of the reduced transition matrix element. For obtaining the hyperfine-induced transition rate, we use the data of levels and the transition rates taken from the Kurucz database [23] and theoretical values of off-diagonal magnetic dipole constants calculated by ourselves.

In the first step, we used the atsp2K program package [24] to estimate the contributions of different intermediate states to the summation in (34). The atsp2K package employs the nonrelativistic multiconfiguration Hartree-Fock (MCHF) approach [22] to calculate the wave function for an atomic state function (ASF), which is expanded in terms of a linear combination of configuration state functions (CSFs),

$$\Psi(\gamma LS) = \sum_j c_j \Phi(\gamma_j LS), \tag{36}$$

where the configuration state functions $\Phi(\gamma_j LS)$ are antisymmetrized linear combinations of products of spin orbitals,

$$\phi_{nlm_l m_s} = \frac{1}{r} P_{nl}(r) Y_{lm_l}(\theta, \varphi) \chi_{m_s}(\sigma). \tag{37}$$

In the MCHF procedure both of the sets of radial functions and the expansion coefficients are optimized to self-consistency. Since CSFs included in the expansion determine the radial functions, they should be selected appropriately. Here the active space method was employed to determine configuration expansions. The idea is to generate CSFs of a specified parity and LS symmetry by electron excitations from one or more reference configurations to an active set of orbitals. The active set was systematically increased in order to monitor the convergence of the calculation. In our calculation, six layers of virtual orbitals, from $n=4$ to $n=9$, with the angular quantum number restricted to $l=4$ or g orbitals were added step by step. A model of single and double excitations (SD) was employed. Configuration expansions were augmented by SD excitations from $4s4p$ valence shells in order to include the valence correlations. Once a set of radial orbitals has been obtained, a Breit-Pauli configuration interaction (BPCI) calculation, where only the expansion coefficients are determined, can be performed to include the relativistic corrections. Then, with these radial orbitals and expansion coefficients, the magnetic dipole constants can be calculated. In Table I, level intervals, transition rates, and off-diagonal magnetic dipole constants are listed for some low-lying γ' states. The phase factors, $p_{\gamma'}$, are determined by the same MCHF procedure. In the last column, the contributions of corresponding intermediate states to the summation in (34) are listed. It shows that only $4s4p\ ^3P_1$ and $4s4p\ ^1P_1$ are dominant, and the contributions of other states can be neglected. We estimated that the truncated error of the hyperfine-induced transition rate is less than 5%.

In the second step, we used the graspVU program package [24] to obtain more accurate theoretical values of the magnetic dipole constants for $4s4p\ ^{3,1}P_1$. The graspVU package employs the relativistic multiconfiguration Dirac-Fock (MCDF) approach to calculate the wave function for an ASF. As in the MCHF approach, the ASF is extended in terms of a linear combination of CSFs,

TABLE I. Calculated values of off-diagonal magnetic dipole constants $A(\gamma', 4s4p\ ^3P_0)$ of ^{67}Zn using the MCHF approach together with the $\varepsilon_{\gamma'}$, level intervals, and transition rates obtained from the Kurucz database [23] for some low-lying immediate states. The phase factors $p_{\gamma'}$ are determined by the same MCHF procedure. The contributions of the corresponding intermediate states to the summation in Eq. (34) are listed in the last column.

γ'	$\varepsilon_{\gamma'}$	$p_{\gamma'}$	$A(\gamma' \rightarrow 4s^2\ ^1S_0)$ (s^{-1})	$A(\gamma', 4s4p\ ^3P_0)$ (MHz)	$E(4s4p\ ^3P_0)-E(\gamma')$ (cm^{-1})	($s^{-1/2}$)
$4s4p\ ^3P_1$	0.9912	+1	2.957×10^4	−554.79	−190.071	+0.01660
$4s4p\ ^1P_1$	0.5747	+1	7.039×10^8	−421.57	−14434.063	+0.01485
$4s5p\ ^3P_1$	0.3829	−1	5.670×10^4	−73.08	−28963.105	−0.000008
$4s5p\ ^1P_1$	0.3681	−1	1.073×10^8	+87.96	−30599.100	+0.00037
$4s6p\ ^3P_1$	0.3270	+1	2.780×10^4	+66.34	−35769.350	−0.000003
$4s6p\ ^1P_1$	0.3232	−1	3.032×10^7	−125.11	−36295.910	−0.00020
Sum						+0.03161

$$\Psi(\gamma J) = \sum_j c_j \Phi(\gamma_j J), \tag{38}$$

but the CSFs, $\Phi(\gamma_j J)$, are jj coupled, and are antisymmetrized linear combinations of products of relativistic orbitals,

$$\phi(\mathbf{r}) = \frac{1}{r}\begin{pmatrix} P_{n\kappa}(r)\chi_{\kappa m}(\hat{\mathbf{r}}) \\ iQ_{n\kappa}(r)\chi_{-\kappa m}(\hat{\mathbf{r}}) \end{pmatrix}. \tag{39}$$

Similar to the case of the MCHF calculation, the active space method and the SD excitation model were employed, and the active set was systematically increased. In the first substep, a Dirac-Fock (DF) calculation was performed to generate the initial radial orbitals for the following calculation. Then, in the second substep, to include valence correlations (VV), configuration expansions were augmented by SD excitations from $4s4p$ valence shells to the virtual set. The virtual set was extended in a similar process as the above MCHF calculations, but the layer was restricted to $n=8$. At the beginning, when only the virtual orbitals of the $n=4$ layer were added, all orbitals were optimized. Thereafter all previously generated orbitals were fixed, and only new orbitals were changed in the self-consistent-field (SCF) procedure. In the third substep, configuration expansions were augmented by SD substitutions from $3s3p3d$ core and $4s4p$ valence shells, but in the case of a double substitution, at most one electron may be excited from core shells. In this way, core-valence correlations (CV) were taken into account. In the SCF procedure, core orbitals obtained from the previous substep were fixed, but all other orbitals were reoptimized layer by layer. After this CV calculation, the magnetic dipole interaction constants A of $^3P_1$ and $^1P_1$ states are 602.71 MHz and 23.367 MHz, respectively (see Table II). They agree with the experimental values well. The absolute deviations from the experimental values are about 6 MHz. However, since the A value of the $^1P_1$ state is small, its relative deviation is large. For improving its accuracy, we redesigned the optimization procedure of orbitals in the CV calculation. In the CSF set, only states of $J=1$ were included, and in the SCF procedure, orbitals of the $n=4$ layer were optimized only for the $^1P_1$ state, while other orbitals were still optimized for both $^3P_1$ and $^1P_1$ states. Then, a CI calculation, where all orbitals are fixed and only expansion coefficients are determined, was performed for the final core-valence expansion in the third

TABLE II. Calculated values of the diagonal and off-diagonal magnetic dipole constants of ^{67}Zn $4s4p\ ^1P_1$, $4s4p\ ^3P_1$, and $4s4p\ ^3P_0$ states using the MCDF approach. The magnetic coupling matrix element $|\langle {}^1P_1|\mu_0|{}^3P_0\rangle|$ is also calculated.

	A (MHz)				$\lvert\langle {}^1P_1\rvert\mu_0\rvert{}^3P_0\rangle\rvert$
Model	$(^3P_1, ^3P_1)$	$(^1P_1, ^1P_1)$	$(^3P_1, ^3P_0)$	$(^1P_1, ^3P_0)$	(μ_B)
DF	492.94	36.446	638.24	457.51	0.0057
VV	474.73	8.883	554.96	420.54	0.0079
VV+CV_1	602.71	23.367	704.17	530.32	0.0093
VV+CV_2	602.40	18.866	714.12	537.63	0.0105
VV+CV+CC	611.91	17.916	748.32	559.14	0.0113
Experiment	609.086(2)[a]	17.7(5)[b]			
Theory[c]	477.6	8.308	−550.5	418.1	

[a]Byron *et al.* [26].
[b]Kowalski and Träger [27].
[c]Marques *et al.* [28].

substep. The results show that $A(^3P_1, ^3P_1)$ did not change remarkably while $A(^1P_1, ^1P_1)$ had been improved. In the final substep, configuration expansions were first augmented by SD substitutions from all $1s2s2p3s3p3d$ core and $4s4p$ valence shells, with the restriction that at most one electron may be excited from core shells, so as to take into account all VV and CV correlations. Then, configurations, generated by double substitutions from the core $3s3p3d$ shells to virtual orbitals of $n=4$, were added to the final CV expansion to include limited core-core (CC) correlations. At last, a CI calculation was performed for these configurations. From Table II, we can see that the values of $A(^3P_1, ^3P_1)$ and $A(^1P_1, ^1P_1)$ agree remarkably well with the experimental values. The corresponding values of $A(^3P_1, ^3P_0)$ and $A(^1P_1, ^3P_0)$ are 748.32 MHz and 559.14 MHz, respectively. Using these values, we can deduce $A_{\mathrm{hfs}}(4s4p\ ^3P_0 \rightarrow 4s^2\ ^1S_0) = 1.550 \times 10^{-2}\ \mathrm{s}^{-1}$ ($\approx 2\pi \times 2.5$ mHz). This 2.5 mHz linewidth is comparable with that of ^{87}Sr (1 mHz [25]) and ^{171,173}Yb (8 mHz, 7 mHz [4]). It is feasible to employ $^1S_0$-$^3P_0$ transition of ^{67}Zn as the clock transition.

Recently, we noticed Marques *et al.* [28] and Liu *et al.* [29] had used the MCDF approach to calculate the decay rate $A_{\mathrm{hfs}}(4s4p\ ^3P_0 \rightarrow 4s^2\ ^1S_0)$ as well. In [28], hyperfine matrix elements were calculated. From those matrix elements, we deduced the hyperfine constants and listed them in the last row of Table II. It seems that Marques *et al.* had neglected so much CV and CC correlations in their calculation that these values were only coincident with our results of VV calculation but far smaller than the experimental values. Using these values, the calculated decay rate will be excessively small. The decay rate that Marques *et al.* obtained was $0.565 \times 10^{-2}\ \mathrm{s}^{-1}$, which was only about one-third of our results. In [29], Liu *et al.* neglected CC correlations and some CV correlations due to electrons of deep core shells, nevertheless, since they had included most of the important correlations, their result ($1.695 \times 10^{-2}\ \mathrm{s}^{-1}$) was quite similar to ours. However, unfortunately, since the off-diagonal magnetic dipole constants were not listed in [29], we could not compare them directly.

Comparing the results in Table II with those in Table I, one may find that the signs of the corresponding off-diagonal magnetic dipole constants are opposite. This is due to the different phase factors of expansion coefficients that were used in two program packages. This difference will not change the relative positive-negative signs between terms in the summation of (34), therefore it will not effect the result of the hyperfine-induced transition rate. Furthermore, this difference will not change the sign of diagonal magnetic dipole constants. $A(^3P_1, ^3P_0)$ obtained from [28] has a different sign than ours in Table II. That should be for the same reason.

IV. $^1S_0$-$^3P_0$ TRANSITION OF BOSONIC ISOTOPES IN APPLIED FIELDS

Though it is convenient to employ the hyperfine-induced $^1S_0$-$^3P_0$ transition in a fermionic isotope, however, this transition in bosonic isotopes has more excellent characters, such as smaller sensitivity to magnetic field and light polarization, and simpler level structure. As mentioned above, this transition in bosonic isotopes is completely forbidden. However, various clever schemes have been proposed to induce the $^1S_0$-$^3P_0$ transition in bosonic isotopes, such as three-photon electromagnetically induced transparency and absorption (EITA) [30], three-level Λ-type EIT [31], static-magnetic-field-induced transition [32,33], phase-matching effect [34], and magic-wave-induced transition [35]. The main idea of these schemes is still to mix or couple the $^3P_0$ state with other states for which electric dipole transition is allowed. Since there is no internal field of atoms to accomplish this purpose, external fields are applied. In the following part of this section, we only interpret some of these schemes briefly and give the corresponding values of Zn. The details of the schemes can be found in the original papers.

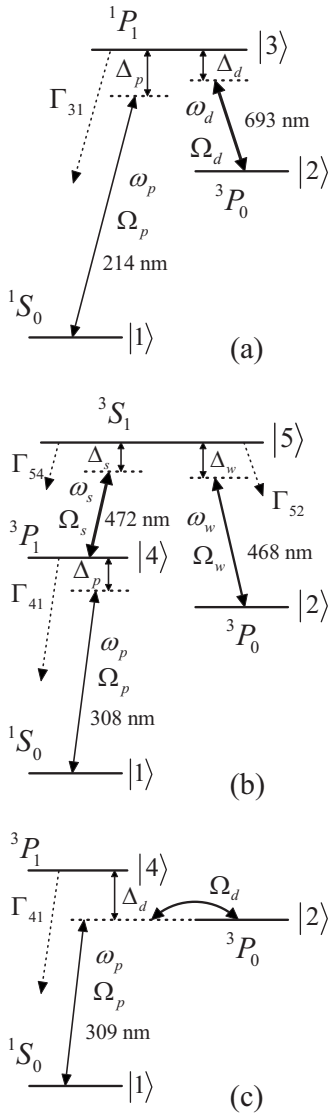

FIG. 6. Energy-level diagrams of Zn related to the schemes of (a) three-level Λ-type EIT, (b) three-photon EITA, and (c) static-magnetic-field-induced transition.

In the scheme of three-level Λ-type EIT [see Fig. 6(a)], $|2\rangle$ $(4s4p\ ^3P_0)$ and $|3\rangle$ $(4s4p\ ^1P_1)$ states are coupled by a

near-resonant laser field (dressing laser), while $|1\rangle$ $(4s^2\ ^1S_0)$ and $|3\rangle$ states are coupled by a weak probe field. Here, both the probe and the dressing lasers are linear polarized, and the electric component of the probe laser and the magnetic component of the dressing laser are aligned along the same axis. When the detuning of the probe laser, Δ_p, is in the vicinity of the detuning of the dressing laser, Δ_d, EIT phenomenon will happen. A narrow dip structure will appear in the broad absorption profile of the $|1\rangle$-$|3\rangle$ transition. When we ignore the decay rate of magnetic-dipole transition $|3\rangle \rightarrow |2\rangle$ and the loss rate of coherence between $|1\rangle$ and $|2\rangle$, the width and the position of the EIT dip are given by

$$\tilde{\Gamma}_1 = \frac{\Omega_d^2}{\Gamma_{31}}, \tag{40}$$

$$\Delta = \Delta_p - \Delta_d = 0, \tag{41}$$

where Γ_{31} is the decay rate of the transition $|3\rangle \rightarrow |1\rangle$, and $\Omega_d = \langle 3|\mu_0|2\rangle B_0/\hbar$ is the Rabi frequency associated with magnetic-dipole (μ_0) coupling of the dressing laser (magnetic amplitude B_0) to the transition $|2\rangle \rightarrow |3\rangle$. The position and the width of the EIT dip is very insensitive with respect to fluctuations of Δ_d, and the difference frequency between the probe laser and the dressing laser can be employed as the frequency standard. Using the above MCDF approach, we also calculated the magnetic coupling matrix element between $|3\rangle$ and $|2\rangle$. Though it was calculated for ^{67}Zn, however, a DF calculation showed that the relative difference of $\langle 3|\mu_0|2\rangle$ between different isotopes is only in an order of 10^{-6}. The final result is $0.0113\mu_B$ (see Table II). With this value, the width of the EIT dip is deduced as

$$\tilde{\Gamma}_1 = 2\pi \times 18.7 I_d, \tag{42}$$

where I_d is the intensity of the dressing laser in mW/cm^2 and $\tilde{\Gamma}_1$ is in units of μHz. As to the ac Stark shift of the clock transition due to off-resonant electric-dipole couplings, only the dressing laser has a significant effect. For $4s^2\ ^1S_0$ and $4s4p\ ^3P_0$ states, the total electronic angular momentums J are zero. Therefore, the dynamic asymmetric and tensor polarizabilities are zero, and the dynamic scalar polarizabilities are given by

$$\alpha_0(4s^2\ ^1S_0) = \alpha_0(4s^2\ ^1S), \quad \alpha_0(4s4p\ ^3P_0) = \alpha_0(4s4p\ ^3P). \tag{43}$$

Ellingsen *et al.* [12] have calculated $\alpha_0(4s^2\ ^1S)$ and $\alpha_0(4s4p\ ^3P)$ for Zn using the time-dependent gauge-invariant (TDGI) method. For dressing laser $(\omega_d = 0.0658$ a.u.), the interpolation values are $\alpha_0(4s^2\ ^1S_0) = 42.86$ a.u., $\alpha_0(4s4p\ ^3P_0) = 86.25$ a.u. Therefore, the ac Stark shifts of $|1\rangle$, $|2\rangle$, and the clock transitions are

$$\Delta\nu_{|1\rangle} = -2.008 I_d, \quad \Delta\nu_{|2\rangle} = -4.040 I_d, \tag{44}$$

$$\Delta\nu_{\text{clock}} = \Delta\nu_{|2\rangle} - \Delta\nu_{|1\rangle} = -2.032 I_d, \tag{45}$$

where I is the intensity of the dressing laser in mW/cm^2 and $\Delta\nu_{|1\rangle,|2\rangle,\text{clock}}$ are in units of mHz. As a numerical example, if a $2\pi \times 0.1$ mHz width of EIT dip is desired, the intensity of the dressing laser should be 5.35 mW/cm^2, and the corresponding ac Stark shift of the clock transition is -10.9 mHz. When the intensity of the dressing laser is stabilized to 1%, the frequency uncertainty induced by the dressing laser will be at the sub-mHz level, corresponding to a fractional frequency uncertainty better than 10^{-18}. The probe laser intensity I_p should also be chosen carefully, since a large intensity may broaden the width of the EIT dip. A probe laser intensity of 10 μW/cm^2 proposed in [31] does not seem to be suitable. In that case, Ω_p, the Rabi frequency associated with coupling of the probe laser to atomic transitions $|1\rangle \rightarrow |3\rangle$, is about 2.2 MHz for Sr, and the width of the EIT dip is broadened to $2\pi \times 3.7$ kHz. In our case of Zn, when $I_p < 1$ pW/cm^2, there is no remarkable broadening effect, but when I_p is 10 pW/cm^2 and 100 pW/cm^2, the width of EIT dip is broadened to $2\pi \times 0.45$ mHz and $2\pi \times 3.8$ mHz, respectively. Thus, one must make a compromise between the width of the EIT dip and the signal amplitude.

In the scheme of the three-photon EITA [see Fig. 6(b)], $|2\rangle$ is coupled with $|5\rangle$ $(4s5s\ ^3S_1)$ by a weak coupling field, and the latter is coupled with $|4\rangle$ $(4s4p\ ^3P_1)$ in turn by a strong coupling field. When $|1\rangle$ and $|4\rangle$ are coupled by a probe laser, the relatively broad absorption line of transition $|1\rangle \rightarrow |4\rangle$ will be suppressed because of the existence of the strong and the weak coupling field. Instead, a narrow EITA line will appear. The width and the position of this EITA line is given by

$$\tilde{\Gamma}_2 = \Gamma_{41} \frac{|\Omega_w|^2}{|\Omega_s|^2}, \tag{46}$$

$$\Delta = \Delta_p + \Delta_s - \Delta_w = (\Delta_s - \Delta_w) \frac{|\Omega_w|^2}{|\Omega_s|^2}, \tag{47}$$

where Γ_{41} is the decay rate of transition $|4\rangle \rightarrow |1\rangle$, Ω_w and Ω_s are the Rabi frequencies associated with couplings of the weak coupling laser and the strong coupling laser to transitions $|5\rangle \rightarrow |2\rangle$ and $|5\rangle \rightarrow |4\rangle$, and Δ_p, Δ_s, and Δ_w are the detuning of the probe, the strong coupling, and the weak coupling fields, respectively. When $|\Delta_s - \Delta_w|$ is small, the algebraic sum of the three laser frequencies, $\omega_p + \omega_s - \omega_w$, is very close to the three-photon resonance, and can be employed as the frequency standard. Γ_{41} of Zn is $2\pi \times 4.71$ kHz. If we assume $\tilde{\Gamma}_2 = 2\pi \times 20$ mHz as in [30], $|\Omega_w|/|\Omega_s|$ should be 2.06×10^{-3} for Zn. The choice of $|\Omega_w|$ and $|\Omega_s|$ is not arbitrary. To suppress the absorption line of transition $|1\rangle \rightarrow |4\rangle$ effectively, $|\Omega_s|$ should be comparable with Γ_{54} and Γ_{52}, the decay rates of transition $|5\rangle \rightarrow |4\rangle$ and $|5\rangle \rightarrow |2\rangle$. Here we choose $|\Omega_s| = \Gamma_{54}$, $|\Omega_w| = 2.06 \times 10^{-3}\Gamma_{54}$. So the corresponding intensities of the strong and the weak coupling laser are 6.0 mW/cm^2 and 78 nW/cm^2, respectively. Similar to the case of the three-level Λ-type EIT scheme, the intensity of the probe laser should be chosen with a compromise between the broadening and the distortion of the sharp absorption peak and the signal magnitude. We found $I_p = 10$ pW/cm^2 is a proper value. In the above calculation, we have assumed only one sublevel in $|4\rangle$ and $|5\rangle$, and ignore any effect of polarization of the light fields

TABLE III. Relevant parameters of the schemes of three-level Λ-type EIT, three-photon EITA, and static-magnetic-field-induced transition for Zn and other alkaline-earth-metal-like atoms.

	Mg	Ca	Sr	Yb	Zn
Three-level Λ-type EIT [31]					
I_d (mW/cm^2)			3.9		5.35
$\tilde{\Gamma}_1/2\pi$ (mHz)			1		0.1
$\Delta\nu_{\text{clock}}$ (mHz)			21		−10.9
Three-photon EITA [30]					
I_s (mW/cm^2)				4	6.0
I_w (nW/cm^2)				10	78
$\tilde{\Gamma}_2/2\pi$ (mHz)				20	20
$\Delta\nu_{\text{clock}}$ (mHz)				10	−10.9
Static-magnetic-field-induced transition [32]					
$\alpha/2\pi$ (Hz/T$\sqrt{\text{mW/cm}^2}$)	98	154	198	186	45.9
$\beta/2\pi$ (MHz/T^2)	−217	−83.5	−23.3	−6.2	−22.9
$\kappa/2\pi$ [mHz/(mW/cm^2)]	−0.5	−3.5	−18	15	10.4
ξ	0.28	0.28	0.30	0.60	0.094

for simplicity as in [30]. The ac Stark shifts of the clock transition due to off-resonant electric-dipole couplings is dominated only by the strong coupling laser (ω_s =0.0965 a.u.). In this case, the dynamic polarizability of $|1\rangle$ is 48.28 a.u. For $|2\rangle$, its off-resonant polarizability cannot be obtained from [12] directly. The contribution of $|5\rangle$ to $\alpha_0(4s4p\ ^3P)$ is $0.118/(0.099\,636^2-\omega^2)$, where 0.118 and 0.099 636 are the values of the oscillator strength and the transition energy for transition $4s4p\ ^3P \rightarrow 4s5s\ ^3S$ calculated in [12]. We excluded it from the values of $\alpha_0(4s4p\ ^3P)$ listed in [12], then, by extrapolation, we obtained the off-resonant polarizability of $|2\rangle$, which is 86.95 a.u. at ω_s=0.0965 a.u. Therefore the ac Stark shift of the clock transition is −10.9 mHz for 6.0 mW/cm^2 intensity of the strong coupling laser. Compared with the three-level Λ-type EIT scheme, the three-photon EITA scheme has an ability of adjusting the width of the clock transition continuously in a large range, but its configuration is more complex and the position of the peak is sensitive to fluctuations of Δ_s and Δ_w. Therefore, for confining the frequency uncertainty induced by coupling lasers, it is necessary to stabilize not only the intensity of the coupling lasers but also their detuning. Assuming the stability of the strong coupling laser intensity to be 1%, the fluctuations of Δ_s and Δ_w should be less than 1 kHz to obtain a fractional frequency uncertainty better than 10^{-17} in our case of Zn.

In [31], Santra *et al.* have indicated that for a large detuning Δ_d of dressing laser, there will be a narrow absorption peak in the vicinity of $\Delta_p=\Delta_d$. When the frequency of the dressing field reduces to zero, the EIT scheme degenerates to the scheme of static-magnetic-field-induced transition [see Fig. 6(c)]. However, since $|4\rangle$ lies much closer to $|2\rangle$ than $|3\rangle$, it will contribute more to the induced transition. Therefore, the main effect of the static magnetic field is to mix $|2\rangle$ with $|4\rangle$ instead of $|3\rangle$, and the Rabi frequency Ω_d is rewritten as $\langle 4|\mu_0|2\rangle B_0/\hbar$ correspondingly. According to the first-order perturbation theory, this new $|2\rangle$ is written as

$$|2\rangle' = |2\rangle + \frac{\Omega_d}{|\Delta_d|}|4\rangle, \tag{48}$$

where $|\Delta_d|$ is equal to the frequency interval between $|4\rangle$ and $|2\rangle$, Δ_{42}, now. Since the transition $|1\rangle \rightarrow |4\rangle$ is weakly allowed, the effective Rabi frequency for excitation of the clock transition is

$$\Omega_{12} = \frac{\Omega_p \Omega_d}{\Delta_{42}}, \tag{49}$$

where $\Omega_p=\langle 4|\mathbf{d}\cdot\mathbf{E}|1\rangle/\hbar$ is the Rabi frequency associated with coupling of the probe laser to atomic transitions $|1\rangle \rightarrow |4\rangle$. In [32], Taichenachev *et al.* have defined coefficients α, β, κ, and ξ as follows:

$$\alpha = \Omega_{12}/\sqrt{I_p}B_0 \cos\theta, \quad \beta = \Delta_B/B_0^2,$$

$$\kappa = \Delta_L/I_p, \quad \xi = \Omega_{12}/\sqrt{|\Delta_L\Delta_B|}\cos\theta, \tag{50}$$

where Δ_B and Δ_L are the induced shifts by magnetic field and probe laser, respectively, and θ is the angle between the linearly polarized $\mathbf{E}$ field of the probe laser and the magnetic field. These coefficients have the relation $\xi=\alpha/\sqrt{|\beta\kappa|}$. Using $\Gamma_{41}=2\pi\times 4.71$ kHz and $\langle 4|\mu_0|2\rangle=\sqrt{2/3}\mu_B$, we obtain α $=2\pi\times 45.9$ Hz/T$\sqrt{\text{mW/cm}^2}$ for Zn. Δ_B is dominated by the contribution of $|4\rangle$ to the second-order Zeeman shift of $|2\rangle$. Thus $\beta=-\Omega_d^2/\Delta_{42}B_0^2=-2\pi\times 22.9$ MHz/T^2. At ω_p =0.1472 a.u., $\alpha_0(|1\rangle)=71.34$ a.u. As to $\alpha_0(|2\rangle)$, we used the finite transition data of lower-lying levels in Kurucz database [23] to estimate roughly, and obtained $\alpha_0(|2\rangle)=-151$ a.u. With these values, we found $\kappa=2\pi\times 10.4$ mHz/(mW/cm^2) and ξ=0.094. Compared with alkaline-earth-metal atoms and Yb, the values of α and ξ for Zn are smaller. This means that for a given spectroscopic linewidth, I_p or B_0 will be larger and the induced shifts will be also larger. However, this scheme is still applicable to Zn. For example, to obtain a induced Rabi frequency of $2\pi\times 0.5$ Hz, we can

choose $B_0=2$ mT and $I_p=30$ mW/cm^2. Assuming the uncertainties of B_0 and I_p are 10^{-7} T and 1%, respectively, as in [32], the combined frequency uncertainty induced by these fields is 9.7 mHz, and the corresponding fractional frequency uncertainty is 10^{-17}.

In the above three schemes, the fractional frequency uncertainties induced by the coupling fields can be controlled below 10^{-17} or even better with realizable conditions, but they contribute only a small part to the total uncertainty. Other effects should also be estimated carefully. However, a complete budget of uncertainties due to various effects is beyond this paper, and will not be discussed here. The scheme using the phase-matching effect is quite similar to the three-level Λ-type EIT scheme, but the lasers interact with atoms in a nonadiabatic regime, instead of adiabatic regime, to obtain a EIT linewidth with a relatively broad linewidth of lasers. As to the scheme of magic-wave-induced transition, the authors have shown its feasibility for Zn. Therefore, we will not discuss these schemes. At last, we list the results of Zn in Table III together with those of alkaline-earth-metal atoms and Yb.

V. CONCLUSIONS

In this paper, we have investigated the laser cooling and trapping of the Zn atom, and various schemes employing the $^1S_0$-$^3P_0$ transition, induced by nuclear magnetic moment or applied fields, as the clock transition. Our numerical simulations showed that Zn can be decelerated by a ZS and captured by a MOT with acceptable parameters. In the strong line MOT, compared with Ca, Sr, and Yb atoms, longer trapping time and more trapping atoms are expected for Zn without using repumping lights since Zn does not have the large $^1P_1$-D-^3P loss channel, and its collisional loss rate due to background gas and coefficient for two-body collisional loss are both smaller. Furthermore, the width of the $^1S_0$-$^3P_1$ transition is adequately wide, and a simple scheme of intercombination line cooling can be employed in the second step to cool Zn atoms to the recoil limit, which has been proved by our 1D semiclassical Monte Carlo simulations. Our calculation results in Sec. III showed that hyperfine-induced $^1S_0$-$^3P_0$ transition of ^{67}Zn is almost as sharp as ^{87}Sr and ^{171,173}Yb and can serve as the clock transition. Meanwhile, the results in Sec. IV showed that different schemes proposed for alkaline-earth-metal atoms and Yb to induce the $^1S_0$-$^3P_0$ transition in bosonic isotopes, including three-photon EITA, three-level Λ-type EIT, and static-magnetic-field-induced transition, can all be applicable for Zn. In conclusion, the Zn atom, either fermionic or bosonic, is a potential candidate for the quantum absorber used in the laser-cooled neutral atomic optical frequency standard. In addition, we also expect a similar conclusion may be drawn for the other group IIB atoms, Cd and Hg.

ACKNOWLEDGMENTS

The authors gratefully acknowledge stimulating discussions with Shuqiang Song and the help of Chun Fan in compiling programs. Atsp2K and graspVU programs were run on the HP Linux Cluster CCSE-I (HP DL360 G4). The authors appreciate the substantial help of the computer center and CCSE of Peking University. This work was supported by the National Natural Science Foundation of China under Grant No. 10474003 and the National Grand Fundamental Research of China (973 program) under Grant No. 2005CB724501.

[1] R. J. Rafac, B. C. Young, J. A. Beall, W. M. Itano, D. J. Wineland, and J. C. Bergquist, Phys. Rev. Lett. **85**, 2462 (2000).
[2] M. Takamoto, F. Hong, R. Higashi, and H. Katori, Nature (London) **435**, 321 (2005).
[3] F. Riehle, H. Schnatz, B. Lipphardt, G. Zinner, T. Trebst, and J. Helmcke, IEEE Trans. Instrum. Meas. **48**, 613 (1999).
[4] S. G. Porsev, A. Derevianko, and E. N. Fortson, Phys. Rev. A **69**, 021403(R) (2004).
[5] O. Kubaschewski and C. B. Alcock, *Metallurgical Thermochemistry, International Series on Materials Science and Technology*, 5th ed. (Pergamon, Singapore, 1989), Vol. 24.
[6] T. Kuwamoto, K. Honda, Y. Takahashi, and T. Yabuzaki, Phys. Rev. A **60**, R745 (1999).
[7] H. J. Metcalf and P. van der Straten, *Laser Cooling and Trapping* (Springer-Verlag, New York, 1999).
[8] T. E. Barrett, S. W. Dapore-Schwartz, M. D. Ray, and G. P. Lafyatis, Phys. Rev. Lett. **67**, 3483 (1991).
[9] T. H. Loftus, T. Ido, M. M. Boyd, A. D. Ludlow, and J. Ye, Phys. Rev. A **70**, 063413 (2004).
[10] X. Xu, T. H. Loftus, J. L. Hall, A. Gallagher, and J. Ye, J. Opt. Soc. Am. B **20**, 968 (2003).
[11] R. D. Cowan, *The Theory of the Atomic Stucture and Spectra* (University of California Press, Berkeley, 1981).
[12] K. Ellingsen, M. Mérawa, M. Rérat, C. Pouchan, and O. Gropen, J. Phys. B **34**, 2313 (2001).
[13] H. C. W. Beijerinck, Phys. Rev. A **61**, 033606 (2000).
[14] E. A. Mason, J. T. Vanderslice, and C. J. G. Raw, J. Chem. Phys. **40**, 2153 (1964).
[15] J. Mitroy and M. W. J. Bromley, Phys. Rev. A **68**, 052714 (2003).
[16] T. P. Dinneen, K. R. Vogel, E. Arimondo, J. L. Hall, and A. Gallagher, Phys. Rev. A **59**, 1216 (1999).
[17] W. J. Meath, J. Chem. Phys. **48**, 227 (1968).
[18] H. Katori, T. Ido, Y. Isoya, and M. Kuwata-Gonokami, Phys. Rev. Lett. **82**, 1116 (1999).
[19] E. A. Curtis, C. W. Oates, and L. Hollberg, Phys. Rev. A **64**, 031403(R) (2001).
[20] T. E. Mehlstäubler, J. Keupp, A. Douillet, N. Rehbein, E. M. Rasel, and W. Ertmer, J. Opt. B: Quantum Semiclassical Opt. **5**, S183 (2003).
[21] W. C. Magno, R. L. Cavasso Filho, and F. C. Cruz, Phys. Rev. A **67**, 043407 (2003).
[22] C. F. Fischer, T. Brage, and P. Jönsson, *Computational Atomic*

Structure, An MCHF Approach (Institute of Physics, Bristol, 1997).
[23] http://cfa-www.harvard.edu/amdata/ampdata/kurucz23/sekur.html
[24] http://www.vuse.vanderbilt.edu/~cff/mchf_collection
[25] H. Kluge and H. Sauter, Z. Phys. **270**, 295 (1974).
[26] F. W. Byron, M. N. McDermott, R. Novick, B. W. Perry, and E. B. Saloman, Phys. Rev. **134**, A47 (1964).
[27] J. Kowalski and F. Träger, Z. Phys. A **278**, 1 (1976).
[28] J. P. Marques, F. Parente, and P. Indelicato, Eur. Phys. J. D **41**, 457 (2007).
[29] Y. Liu, R. Hutton, Y. Zou, M. Andersson, and T. Brage, J. Phys. B **39**, 3147 (2006).
[30] T. Hong, C. Cramer, W. Nagourney, and E. N. Fortson, Phys. Rev. Lett. **94**, 050801 (2005).
[31] R. Santra, E. Arimondo, T. Ido, C. H. Greene, and J. Ye, Phys. Rev. Lett. **94**, 173002 (2005).
[32] A. V. Taichenachev, V. I. Yudin, C. W. Oates, C. W. Hoyt, Z. W. Barber, and L. Hollberg, Phys. Rev. Lett. **96**, 083001 (2006).
[33] Z. W. Barber, C. W. Hoyt, C. W. Oates, L. Hollberg, A. V. Taichenachev, and V. I. Yudin, Phys. Rev. Lett. **96**, 083002 (2006).
[34] D. Yu and J. Chen, Phys. Rev. Lett. **98**, 050801 (2007).
[35] V. D. Ovsiannikov, V. G. Pal'chikov, A. V. Taichenachev, V. I. Yudin, H. Katori, and M. Takamoto, Phys. Rev. A **75**, 020501(R) (2007).